Experimental study of ${}^{12}_{\Lambda}C$ proton weak decay with FINUDA

by
YongJin Lee

February 2007

Department of Physics
Graduate School
Seoul Nation University

Abstract

We have recently measured the non-mesonic weak decay(NMWD) proton spectrum of Λ hypernucleus at FINUDA. The main reaction is $(K^-, \pi^-)^{12}_{\Lambda}$C. There are two decay modes in the NMWD. One is $\Lambda + n \rightarrow n + n$ and the other is $\Lambda + p \rightarrow n + p$. The theoretical and experimental Γ_n/Γ_p ratio is not same. To solve this puzzle, FINUDA experiment was performed. Because E462 experiment's setup could detect the events using coincidence measurements, we can get the Γ_n/Γ_p ratio without FSI effects.

Contents

List of Figures

List of Tables

Chapter 1

Introduction

1.1 Overview

A hypernucleus is a many-body system composed of conventional non-strange nucleus(protons and neutrons) and one or more strange baryons(the Λ , Σ, Ξ). Because Λ is the lightest strange baryon which consists of u, d and s quarks, a Λ hypernucleus is the easiest hypernuclear system to investigate and its structure has been studied quite well. The presence of this new strangeness degree of freedom in a hypernucleus adds a new dimension to the evolving picture of nuclear physics.

1.2 Weak decay of Λ hypernuclei

A Λ hyperon can be used as a unique probe to investigate interior of nuclei. It penetrates deep inside the nucleus because it does not suffer from the Pauli exclusion principle due to the new degree of freedom, *"strangeness"*.

The Λ hyperon produced inside a nucleus via a reaction like, (π^+, K^+) or (K^-, π^-), will de-excite to a hypernuclear ground state which is stable hadronically and electromagnetically and will eventually decay through a strangeness changing weak interaction process which involve the emission of pion or nucleons [20].

A free Λ hyperon decays mostly into a nucleon and a pion via the mesonic

weak decay

$$\Lambda \to \begin{cases} p + \pi^- + 37.8 \text{ MeV} & (63.9\%) \\ n + \pi^0 + 41.1 \text{ MeV} & (35.8\%) \end{cases}$$

with the life time of 263.2 ps [21].

The branching ratios of two channels are 36% and 64% and it is well matched with the simple calculation from the empirical $\Delta I = 1/2$ rule. The energy released in the free decay is about 40 MeV and the corresponding momentum of nucleon and pion in their c.m. frame is about ~ 100 MeV/c.

When a Λ is bound in the nucleus, the mesonic decay channel is suppressed except for the very light nuclei because of Pauli blocking of the final-sate nucleon. The nucleon-induced decay, so called nonmesonic weak decay (NMWD), becomes dominant which is not available to the free Λ [22].

$$\begin{aligned} \Lambda + p &\to p + n + 176 \text{ MeV}, \\ \Lambda + n &\to n + n + 176 \text{ MeV}. \end{aligned}$$

Thus, the total weak decay width(Γ_{tot}) of a Λ hypernucleus consists of four partial decay widths:

$$\Gamma_{tot} = \frac{1}{\tau_{HY}} = \begin{cases} \Gamma_m = \begin{cases} \Gamma_{\pi^-} & \Lambda \to p + \pi^- \\ \Gamma_{\pi^0} & \Lambda \to n + \pi^0 \end{cases} \\ \Gamma_{nm} = \begin{cases} \Gamma_p & \Lambda + p \to n + p \\ \Gamma_n & \Lambda + n \to n + n \\ \Gamma_{2N} & \Lambda + N + N \to N + N + N(?) \end{cases} \end{cases} \quad . \tag{1.1}$$

where τ_{HY} is the lifetime of a hypernucleus and $\Gamma_{\pi^{-(0)}}$ is the partial decay width of $\pi^{-(0)}$-mesonic decay and $\Gamma_{p(n)}$ that of the proton(neutron)-induced NMWD, respectively. The new decay mode of NMWD, two-nucleon ($2N$) induced process ($\Lambda NN \to NNN$), was suggested by Alberico [23], where the virtual pion emitted at the weak vertex is absorbed by pair of nucleons which are correlated through the strong force. Ramos made a more realistic calculations and their calculations showed that the contribution of two nucleon induced process is 20-30% of the free Λ width [24]. However, so far we have no experimental evidence of the $2N$ process.

The nucleon-nucleon (NN) interaction has been extensively studied since the 1930's based on a large amount of NN scattering data and is fairly

well-established theoretically. For unified understanding of extended "baryon-baryon" interaction, there have been interests in the hyperon-nucleon (YN) and the hyperon-hyperon (YY) interactions. The direct measurement of YN and YY interactions by scattering experiment is difficult due to the short life-time and the low intensity of the hyperon beam. Thus, those interactions have been studied in the hypernuclear experiments. The studies of the mesonic and NMWD of the Λ hypernucleus have brought fruitful knowledge to the understanding of the strong and weak ΛN interactions.

Recent review article [25] described the details of the various models and their results on NMWD widths.

1.2.1 Mesonic weak decay

The released energy in the mesonic decay mode is $Q^{free} \simeq 37$ MeV, with a release of kinetic energy of about 5 MeV to the nucleon, corresponding to a final momentum of about 100 MeV/c. Since the nucleon Fermi momentum in usual nuclei is $k_F \simeq 270$ MeV/c except for light ones, the mesonic decay mode is suppressed in heavier hypernuclei because of Pauli exclusion principle of the final-state nucleon.

Although the partial decay width is very small (less than 1%) [26], the mesonic decay is observed in the finite nuclei. The momentum of Λ in its ground state is not zero, which gives the nucleon chances to have larger momentum than Fermi momentum. Furthermore, the local Fermi momentum becomes smaller near the nuclear surface, which also gives the Λ more chances to decay through the mesonic channel. The pion properties are strongly renormalized in the nuclear matter. The mesonic decay width with the distorted pion wave function is larger than that without distortion effect because of the enhancement of the high-momentum component of the wave function in momentum space. Therefore, the partial decay width and the energy distribution of the mesonic decay would probe the theoretical models for hyernuclear structure and pion propagation in the nuclear medium.

A further interesting prediction for the mesonic decays is the remarkable shell effect and charge dependence of the decay width for p-shell and s-shell hypernuclei. For example, the π^- decay width is even weaker than the π^0

decay width in case of . However, for , the π^- decay is four times as strong as the π^0 decay. The calculated $\Gamma_{\pi^0}/\Gamma_{\pi^-}$ ratios of *p*-shell and *sd*-shell hypernuclei vary from a minimum of ~ 0.1 to a maximum of ~ 2.3 [27].

1.2.2 $\Delta I = 1/2$ rule

Another physics interest is the empirical $|\Delta I| = 1/2$ rule, which approximately hold well in the decay of hyperons and kaons. A free Λ decay via the pionic channel :

$$\Lambda \rightarrow \begin{cases} p + \pi^- \\ n + \pi^0 \end{cases}$$

with the experimental ratio of the relevant width, $\Gamma_{\pi^-}/\Gamma_{\pi^0} \simeq 1.78$. We note that, since the nucleon and pion can only combine to give total isotopic spin $I = \frac{1}{2}$ or $\frac{3}{2}$ while the I-spin of the Λ zero, therefore the I-spin cannot be conserved in this process. Gell-Mann suggested that the change in I-spin would be the minimum possible, i.e.

$$|\Delta I| = \frac{1}{2}$$

We can write I-spin wave functions for $(p\pi^-)$ and $(n\pi^0)$ in terms of the I-spin $\frac{1}{2}$ and $\frac{3}{2}$ wave function using the Clebsch-Gordan coefficients.

$$\begin{aligned} |p\pi^-\rangle &= \sqrt{\frac{1}{3}}|\frac{3}{2}\rangle - \sqrt{\frac{2}{3}}|\frac{1}{2}\rangle \\ |n\pi^0\rangle &= \sqrt{\frac{2}{3}}|\frac{3}{2}\rangle + \sqrt{\frac{1}{3}}|\frac{1}{2}\rangle. \end{aligned}$$

The relations then give for the decay ratio

$$\frac{\Lambda \rightarrow p\pi^-}{\Lambda \rightarrow n\pi^0} = \begin{cases} 2:1 & \text{for I} = \frac{1}{2} \quad \text{i.e. } \Delta\text{I} = \frac{1}{2} \\ 1:2 & \text{for I} = \frac{3}{2} \quad \text{i.e. } \Delta\text{I} = \frac{3}{2} \end{cases} \tag{1.2}$$

A small correction for the slightly different phase space available in the two decays change the $I = \frac{1}{2}$ ratio from 2:1 to 1.90:1 to be compared with the experimentally measured 1.78:1. Some further small corrections for electromagnetic effects bring the measured and calculated numbers into good agreement.

This $\Delta I = 1/2$ enhancement, known as the "$\Delta I = 1/2$ rule", is not expected naively in the standard model of the weak interaction. There has been a great deal of theoretical work attempting to identify the origin of this results [28]. However, the origin of this empirical rule is essentially not understood in a fundamental way.

Furthermore, it is not at all clear whether the $\Delta I = 1/2$ rule, which governs the pionic decay of the Λ, should play any role in the NMWD process. There are some indications that it could be violated for the $\Lambda N \to NN$ process. In many references, the authors persisted that they saw the violation of $\Delta I = 1/2$ in NMWD $\Lambda N \to NN$ process [29, 30, 31].

1.2.3 Nonmesonic weak decay

The possibility of nonmesonic weak decay (NMWD) in hypernuclear decay was suggested for the first time in 1953 [32] and interpreted in terms of the free space $\Lambda \to \pi N$ decay, where the pion was considered as virtual and then absorbed by a bound nucleon.

Although the free hyperon-nucleon interaction can be directly measured, experiments are really difficult due to the short lifetime and the low intensity of the hyperon beam. The production and scattering should take place in the same target. Angular distributions and polarizations have been measured at a few energies, particularly for the ΛN system, but the statistics are very poor and imprecise [28, 33]. Therefore, NMWD provides the most practical means to investigate the four-fermion weak vertex and $\Lambda N \to NN$ weak interaction which occurs only in the nuclear medium.

As mentioned in Section 1.2.1, the mesonic decay in the nuclear medium is strongly suppressed because of Pauli blocking effect except for the lightest hypernuclei. The energy released in the NMWD process is $Q^{free} \simeq 176$ MeV, and the corresponding c.m. momentum of final two nucleons is about 400 MeV/c which is much higher than Fermi momentum. As a result, this decay mode does not suffer from Pauli suppression so seriously and dominates in medium and heavy hypernuclei.

The NMWD is expected to contain rich information about the baryon-baryon weak interaction since both parity-conserving (PC) and parity-violating

Table 1.1: NMWD amplitude from ΛN S-state.

Initial Λ N		Final NN	Amplitude $\Lambda p \to np$	Amplitude $\Lambda n \to nn$	Isospin I_{NN}	Parity Change
$^1S_0$	$\to$	$^1S_0$	a_p	a_n	1	no
	$\to$	$^3P_0$	$b_p\frac{1}{2}(\sigma_1-\sigma_2)q$	$b_n\frac{1}{2}(\sigma_1-\sigma_2)q$	1	yes
$^3S_1$	$\to$	$^3S_1$	c_p		0	no
	$\to$	$^3D_1$	$d_p\frac{\sqrt{2}}{4}S_{12}(q)$		0	no
	$\to$	$^1P_1$	$e_p\frac{\sqrt{3}}{2}(\sigma_1-\sigma_2)q$		0	yes
	$\to$	$^3P_1$	$f_p\frac{\sqrt{6}}{4}(\sigma_1+\sigma_2)q$	$f_n\frac{\sqrt{6}}{4}(\sigma_1+\sigma_2)q$	1	yes

(PV) partial rates can be measured, whereas the strong interaction masks the PC signals of the weak interaction in the nucleon-nucleon system. The parity-conserving part of the weak interaction is not observable because it is completely covered by the strong interaction and only the parity-violating part can be studied through the polarization study of interaction. In the case of $\Lambda N \to NN$ interaction, both the parity-conserving and parity-violating parts are observable because the $\Lambda N \to NN$ is completely weak process. Because the relative ΛN momentum is fairly small, the ΛN initial state is restricted to S-state. Then, the possible transitions are those listed in Table 1.1. All amplitudes(a-f) can contribute to the proton-induced NMWD (Γ_p). Three amplitudes(c,d and e) have isospin $I = 0$ in the final NN system which give no contribution to the neutron-induced decay process. Since proton-neutron system has an isospin either 0 or 1, the six amplitudes contribute to the proton-induced decay process. The decay widths Γ_p and Γ_n are written as

$$\begin{aligned}\Gamma_p &= a_p^2 + b_p^2 + c_p^2 + d_p^2 + e_p^2 + f_p^2,\\ \Gamma_n &= a_n^2 + b_n^2 + f_n^2.\end{aligned}$$

If the $\Delta I = 1/2$ rule holds in the NMWD. the relations of the amplitudes of $\Lambda p \to np$ and $\Lambda n \to nn$ are

$$\begin{aligned}a_n &= \sqrt{2}a_p,\\ b_n &= \sqrt{2}b_p,\end{aligned}$$

$$f_n = \sqrt{2} f_p.$$

Then, the Γ_n/Γ_p ratio can be written as,

$$\frac{\Gamma_n}{\Gamma_p} = \frac{2\Gamma(I=1)}{\Gamma(I=0)+\Gamma(I=1)} \tag{1.3}$$

When the $\Delta I = 1/2$ rule holds and if the initial state is the singlet spin state $^1S_0$, then the ratio of neutron- to proton-induced transitions to final $I = 1$ states is $\Gamma_n(I=1)/\Gamma_p(I=1) = 2$. Therefore, by isolating the initial singlet spin state $^1S_0$, which leads to only $I = 1$ states, both in neutron- and proton-induced decays, the validity of the $\Delta I = 1/2$ rule in the NMWD could be verified.

1.3 FINUDA Experiment

1.3.1 The measurement of Γ_n/Γ_p

Table 1.2 shows the difference between experimental and theoretical result for Γ_n/Γ_p . To solve this problem, we performed the FINUDA experiment.

We simultaneously measured two nucleons (n + p, n + n) from decay of Λ hypernucleus. The advantage of the coincidence experiment is that we can remove both of the difficulty and uncertainty.

It should be noted that the Γ_n/Γ_p ratio can be determined directly without any assumption as follows.

$$\begin{aligned} \mathrm{N}(np\text{- pair coin.}) &= \mathrm{N}(\Lambda p \to np) \times (\Omega_p \times \Omega_n)_{av.} \times \epsilon_n \times \epsilon_p \times (1 - R_{FSI}) \\ \mathrm{N}(nn\text{- pair coin.}) &= \mathrm{N}(\Lambda n \to nn) \times (\Omega_n \times \Omega_n)_{av.} \times \epsilon_n^2 \times (1 - R'_{FSI}) \end{aligned}$$

where $(\Omega_p \times \Omega_n)_{av.}/(\Omega_n \times \Omega_n)_{av.}$ and ϵ_p/ϵ_n denote averaged acceptance of decay counter for n-p/n-n pair and detection efficiencies of proton/neutron, respectively. R_{FSI} stands for the reduction factor due to the FSI. Then the ratio of Γ_n/Γ_p is expressed as;

$$\frac{\Gamma_n}{\Gamma_p} \equiv \frac{\mathrm{N}(\Lambda n \to nn)}{\mathrm{N}(\Lambda p \to np)} = \frac{\mathrm{N}(n+n\text{ - pair coin.})}{\mathrm{N}(n+p\text{ - pair coin.})} \times \frac{\epsilon_p}{\epsilon_n} \tag{1.4}$$

The FSI factor is canceled out due to the charge symmetry between proton and neutron. This experiment can precisely deduce the Γ_n/Γ_p ratio without theoretical ambiguity of the FSI effect.

Table 1.2: Recent theoretical calculations and experimental results of Γ_n/Γ_p ratio for .

Theoretical results

Ref.	Γ_n/Γ_p	Model
Ramos-Bennhold [51]	0.19	OPE
	0.27	OME
Parreno [52]	0.12	OPE
	0.12	$\pi + \rho$
Dubach [53]	0.20	OPE
	0.83	OME
Parreno [39]	0.104	OPE
	0.095	$\pi + \rho$
	0.068	OME
Parreno [54]	0.68	OME
	0.034-0.136	OME + $\Delta I = 3/2$
Itonaga [56]	0.10	OPE
	0.36	$\pi + 2\pi/\rho + 2\pi/\sigma$
Jun [57]	0.08	OPE
	1.14	OPE + 4BPI
Jido [45]	0.12	OPE
	0.52	$\pi + K$
	0.53	$\pi + K + 2\pi + \omega$
Parreno-Ramos [40]	0.078-0.079	OPE
(correction of [39])	0.205-0.343	$\pi + K$
	0.288-0.341	OME

Experimental results

J. J. Szymanski [58]	$1.33^{+1.12}_{-0.81}$
H. Noumi [64]	$1.87^{+0.67}_{-1.16}$
O. Hashimoto [60]	$1.17^{+0.09+0.20}_{-0.08-0.18}$(1N only)
	$0.96^{+0.10+0.22}_{-0.09-0.21}$(1N and 2N)
Y. Sato [59]	$0.87 \pm 0.09 \pm 0.21$(1N only)
	$0.60^{+0.11+0.23}_{-0.09-0.21}$(1N and 2N)
J. H. Kim [63]	0.51 ± 0.15(1N)

Chapter 2

FINUDA experiment

The FINUDA (acronym for" FIsica NUcleare a DAΦNE") experiment is a multi- purpose experiment mainly focused on hypernuclear physics. The topics to study in this experiment are listed below;

- Λ-hypernuclear spectroscopy with the $(K^-_{Stopped}, \pi^-)$ reaction,
- Lifetime measurement of Λ-hypernuclei,
- Weak decay of Λ-hypernuclei,
- Search for rare decays of ${}^{4}_{\Lambda}$He into p + t or d + d,
- Neutron-rich hypernuclear formation with the $(K^-_{Stopped}, \pi^-)$ reaction,
- Search for Σ-hypernuclei with the $(K^-_{Stopped}, \pi^{\pm})$ reaction.

The main idea [27-29] is to use almost monochromatic slow K^-'s from the decay of $\phi(1020)$, which is abundantly produced by the ϕ factory DAΦNE [30] at LNF(Laboratori Nazionali di Frascati). They are slowed down while passing through inner detectors and targets until they stop inside the targets. When a negative kaon stops, it is captured by an atomic orbit of a nucleus, cascading down to lower orbitals, until absorbed by one or more surface nucleons of the nucleus. It is well known from the old bubble chamber data [31] that the main

absorption process (80-85% per stopped K^-) is the quasi-free process,K^-N $\rightarrow \Lambda\pi$ and K^-N $\rightarrow \Sigma\pi$, while non-mesonic absorption processes, K^-NN $\rightarrow \Lambda$ (Σ)N, on multi-nucleons take place with a significant fraction of 15-20 % in a wide range of mass number. Some of the Λ-hypernuclei as

$$\mathrm{K}^-_{Stopped} + {}^{A}\mathrm{Z} \rightarrow {}^{A}_{\Lambda}\mathrm{Z} + \pi^- \tag{2.1}$$

The measurement of the momentum of the emitted pion gives us information on the mass of the formed hypernuclear states.

Λ hypernuclei decay via weak interaction with the lifetime comparable to that of a Λ hyperon in free space (263 $\pm$ 2 ps). It involves one or more neighboring nucleons in its decay except for light hypernuclei. The ratio between neutron-induced ($\Lambda N \rightarrow NN$) and proton-induced ($\Lambda p \rightarrow pp$) decay widths, denoted as Γ_n/Γ_p, imposes restrictions on the baryon-baryon weak interaction models. Not only the direct formation of reaction (2.1), but also a fragment of hyper-nucleus (hyperfragment) is produced sometimes. In particular, ${}^{4}_{\Lambda}$Heis abundantly produced with a ^{6}Li target, since lam is particle-unstable and decays into ${}^{5}_{\Lambda}He$ + p, ${}^{4}_{\Lambda}$He+ p + n , ${}^{4}_{\Lambda}$He+ n + n and so on, according to the excitation energy of lam. The specific non-mesonic two-body decays of ${}^{4}_{\Lambda}$Heinto p + t and d + d have not been observed yet. In the large-angle spectrometer FINUDA we expect to observe p + t or d + d pair in back-to-back with a good energy resolution. Simultaneously, the FINUDA experiment supplies us information on the formation of neutron-rich hypernuclei (which have never been observed with the stopped K^- method up to now) from the following reaction:

$$\mathrm{K}^-_{Stopped} + {}^{A}\mathrm{Z} \rightarrow {}^{A}_{\Lambda}(\mathrm{Z}\text{ - }2) + \pi^+ \tag{2.2}$$

For example, ${}^{6}_{\Lambda}H$, ${}^{7}_{\Lambda}H$ and ${}^{12}_{\Lambda}Be$ can be produced with ^6Li, ^7Li and ^{12}C targets, respectively. Another kind of hypernucleus, which includes one Σ hyperon, is also looked for, by tagging a particle emitted from in the strong conversion process of ΣN$\rightarrow\Lambda$N.

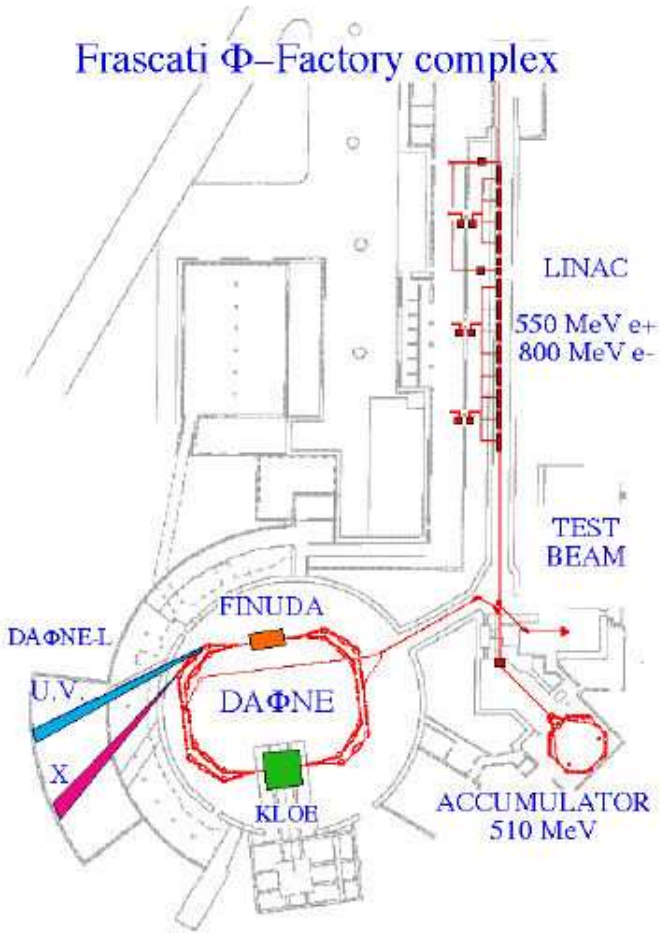

Figure 2.1: Schematic layout of the DAΦNE accelerator complex.

energy	510MeV
design luminosity	$5 \times 10^{32}/\mathrm{cm}^2/\mathrm{s}$
σ_x(rms)	2.11 mm
σ_y(rms)	0.021mm
σ_z(rms)	35mm
bunch length	30mm
crossing angle	13mrad
frequency (max)	368.25MHz
bunch/ring	up to 120
particles/bunch	8.9×10^{10}
current/ring(max)	5.2A

Table 2.1: Operation parameters of the DAΦNE collider.

2.1 DAΦNE

The ϕ factory DAΦNE, which is the acronym for "the Double Annular Φ Factory for Nice Experiment", is a positron-electron collider whose beam energy is 0.510GeV so that the center-of-mass energy corresponds to the ϕ (1020) mass. The main decay modes of a ϕ meson is K^+K^- (49%), K_LK_S (34 %) and $\rho\pi^0$ + $\pi^+\pi^-\pi^0$ (15%).

The operation parameters are listed in Table 2.1. As shown in Fig. 2.1, the DAΦNE collider has two colliding sections; one for the KLOE experiment on kaon decays and the other for the FINUDA experiment.

2.2 FINUDA spectrometer

Figure 2.2 shows a global view of the FINUDA spectrometer. ϕ mesons are produced by in the center of this apparatus. A homogeneous magnetic field of 1.0 T is applied along the beam pipe with a superconducting solenoid.

The FINUDA spectrometer is composed of two regions: the internal target region and external region.

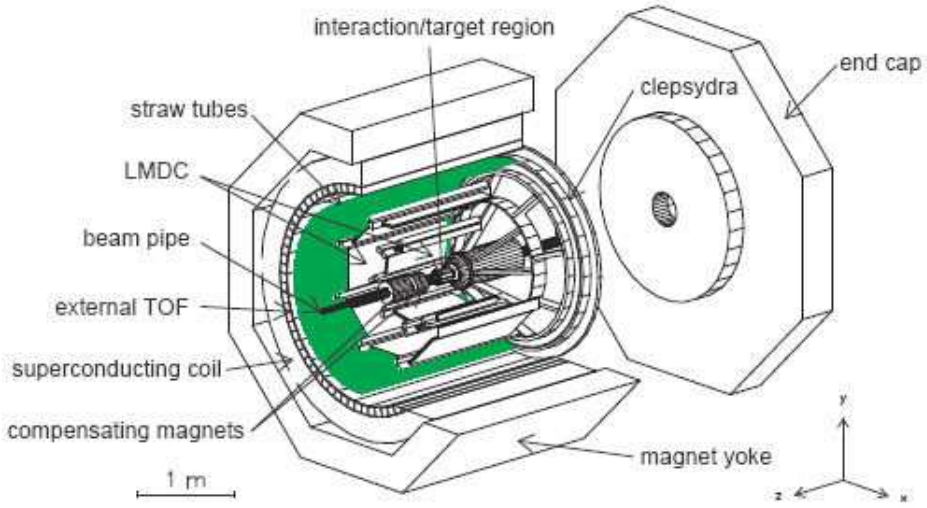

Figure 2.2: Global view of the FINUDA spectrometer.

2.2.1 Inner detectors

A $K^{\pm}$ pair from the ϕ decay is detected in the internal region, shown in Fig. 2.3, with a barrel of 12 thin scintillator slabs (TOFINO) and an octagonal array of silicon microstrips (ISIM).

The slow $K^{\pm}$ are identified with the large energy deposit in ISIM, compared to minimum ionizing particle, e.g. $e^{\pm}$, mainly coming from Bhabha scattering (Fig. 2.4). The TOFINO is used to make a trigger start timing. At this stage of analysis, the timing resolution of ∼610 ps is achived. Each slab of the TOFINO is 20cm long, 3.1cm wide, and 2.3mm thick.

The $K^{\pm}$ stopping points are estimated with the hits in ISIM. Here, the decay topology of $\phi \rightarrow K^{+}K^{-}$ is assumed for the trajectories. Each module of ISIM has an active surface of 196mm × 52mm with strips on both sides (z and ϕ). The pitch between the neighboring strips is 50μm. The present resolution is evaluated to be $\sigma_Z \sim 30\mu$m

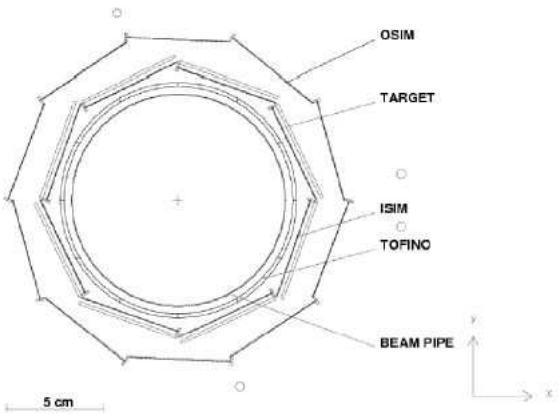

Figure 2.3: Schematic view of the interaction/target region.

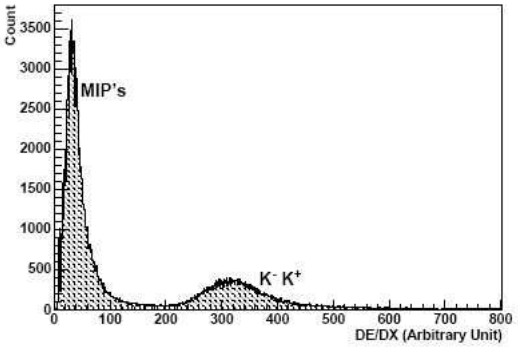

Figure 2.4: Energy deposit in ISIM > MIP‘s and kaons are clearly separated.

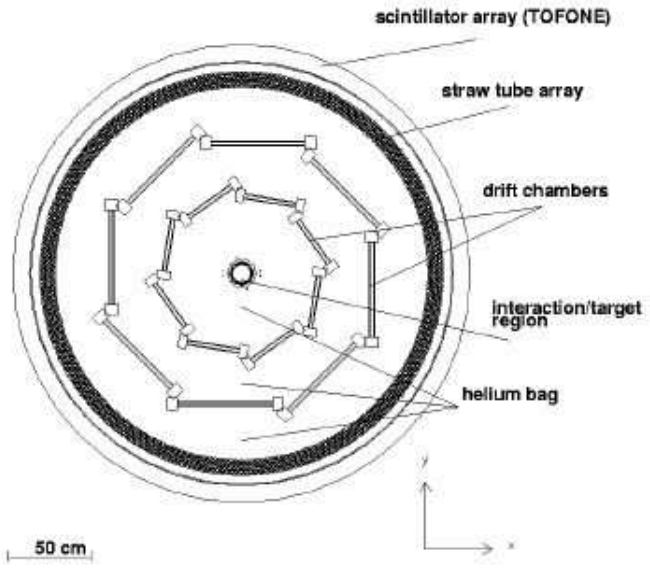

Figure 2.5: Front view of the FINUDA spectrometer.

2.2.2 Outer detectors

A front view of the spectrometer is shown in Fig.2.5. Four sets of position detector systems are used to track a particle from a target. First one is a decagonal array of silicon microstrips (OSIM) which are the same as ISIM, then two layers of eight low mass drift chambers (DCH1, DCH2) are located. The outermost one is a straw tube detector(STRW) consisting of six layers longitudinal and stereo tubes. The whole tracking volume is filled with He gas to reduce the effect of multiple scattering.

DCH1 and DCH2 are rotated by 11° and the lateral sides of the frames are overlapped for a negative particle of $\sim$ 250 MeV/c. They are filled with a gas mixture of He : iso - C_4H_{10} = 70 % : 30 % to reduce the radiation length. The sensitives areas for DCH1 and DCH2 are 930mm $\times$ 316mm and 1570mm $\times$ 566mm, respectively. The sense wire pitch is 50mm. The spatial resolution in the direction normal to the wire is assumed to be $\sigma = 150\mu$m, while the

resolution along the wire of 1% of the wire length can be obtained by charge division.

The straw tube arrays are composed of one axial and two stereo (tilted by 12°) super-layers. Each super-layer contains two layers of staggered straws. The inner diameter of a straw is 15mm and the length is 2.55m. The resolution along the drift is expected to be 100μm. To attain a good resolution for z-direction, the z coordinate is evaluated with the stereo tubes. Then, the resolution for z direction becomes $\sim$ 500μm.

There are an external barrel of 72 scintillator slabs (TOFONE) in the outermost, used for the first level trigger together witho TOFINO. The time-of-flight between TOFINO and TOFONE is used for the particle identification for charged particles and the detection of neutrons. Each slab is 255 cm long and 10 cm thick. The section is shaped as a trapezoid with the upper base of 12 cm and the lower base of 11 cm. The time resolution is estimated to be $\sim$ 770ps at present, by timing alignment using cosmic rays and Bhabha scattering data.

2.2.3 Particle identification

We have to identify π^+/p/d for positive particles. We have information on the energy deposit at OSIM and the time-of-flight. Figure 2.6 shows the scatter plot between the momentum and the energy deposit; π^+, p and d are separated very clearly.

2.2.4 Targets

In the first run in 2003 and 2004, we used five kinds of targets (2$\times^6$Li, ^{7}Li, 3$\times^{12}$C, ^{27}Al and ^{51}V). Each target has its thickness of 200-300 mg/cm^2. Each target has the following purposes.

^{6}Li: The hypernucleus lam is particle-unstable and decays into ${}^{5}_{\Lambda}He$, or ${}^{4}_{\Lambda}He$. The study on weak decay for ${}^{5}_{\Lambda}He$ and the two-body rare decay for and ${}^{4}_{\Lambda}He$ is possible. Furthermore, a neutron-rich hypernucleus is possibly produced and even if no signal is observed we will determine the upper limit on the formation rate.

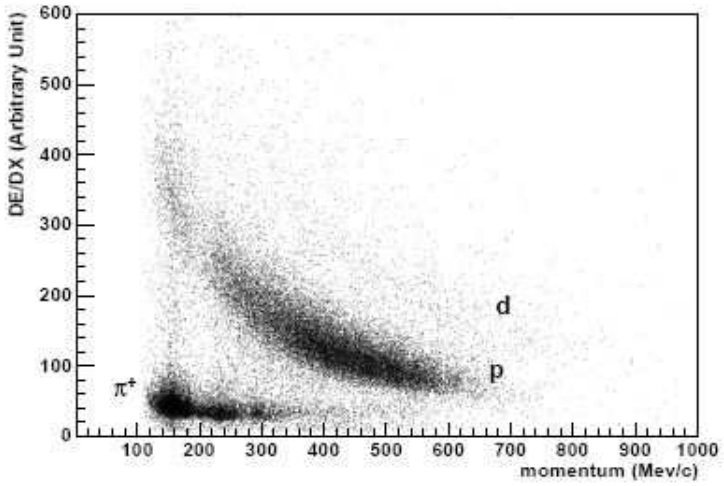

Figure 2.6: Energy deposit at OSIM versus particle momentum. Pions, protons and deuterons are clearly separated.

^{7}Li: The level scheme of am is well known by the high-resolution γ spectroscopy. The groun state doublet will be resolved in the missing-mass spectroscopy for the first time. The weak decay of this hypernucleus can be measured. The possible existence of ${}^{7}_{\Sigma}$Li (theoretically most promising except for ${}^{4}_{\Sigma}$He, which was observed already) and neutron-rich hypernucleus ${}^{7}_{\Sigma}$He,can be surveyed.

^{12}C: ${}^{12}_{\Lambda}C$ has been studied most extensively up to now, with the (K^-, π^-) and (π^+, K^+) reactions. We can use the previous spectra for calibration, and also we will have a spectrum with the best resolution (0.75MeV FWHM), compared to the present record of 1.45MeV FWHM at the KEK-PS E369 experiment.

^{27}Al: and ^{51}V No distinct hypernuclear state has been observed heavier than ${}^{16}_{\Lambda}$O with stopped K^-. The capture rate for ${}^{27}_{\Lambda}$Al and ${}^{51}_{\Lambda}$V will be measured.

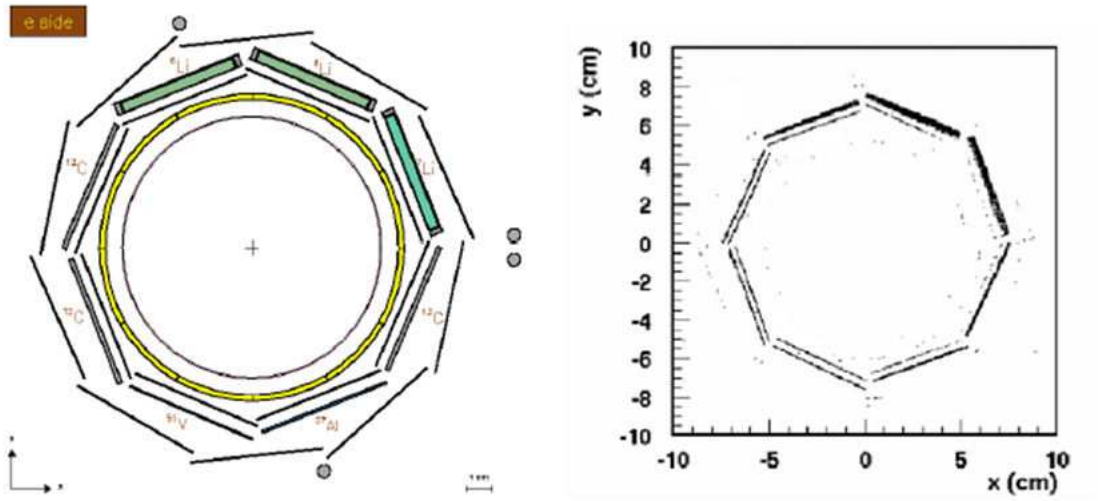

Figure 2.7: (a) Schematic view of the interaction/target region. (b) Scatter-plot of the reconstructed y vs x coordinates of the K^- stopping points.

2.2.5 Trigger

For the $(K^-_{stopped}, \pi^-)$reaction, we make a trigger as follows.

As a ϕ decay selection, we require two "extended" back-to-back hists fo the TOFINO slabs with the ADC's over the kaon threshold. "Extended" means that one hit is just opposite or adjacent to the opposite. This is because the magnetic field bends the kaon trajectories. We also require more than two hits in the TOFONE slabs, of which the first hit is within the time gate(18ns) after the hits in TOFINO. Most of the pions from hypernucleus formation pass through more than two slabs in TOFONE because of the curvature of the pion track.

For the luminosity monitor, we have a Bhabha trigger. It is produced as in the ϕ decay selection but with the small pulse heights in TOFINO.

2.3 Acceptance of charged particles

We have the acceptance for charged particles as shown in Fig.2.7. Since the spectrometer is optimized for the π^- from hypernucleus formation (260 - 280 MeV/c), negative particles have a larger detection acceptance than positive ones. The frames of drift chambers are rotated between the inner and outer layers, so that the inefficiency for a negative particle is reduced. A track with four hits in detectors (OSIM-DCH1-DCH2-STRW), called a long track has an acceptance in $\geq$ 150 MeV/c, and a short track with three hits in detector (OSIM-DCH1-DCH2) has an acceptance in $\geq$ 120 MeV/c.

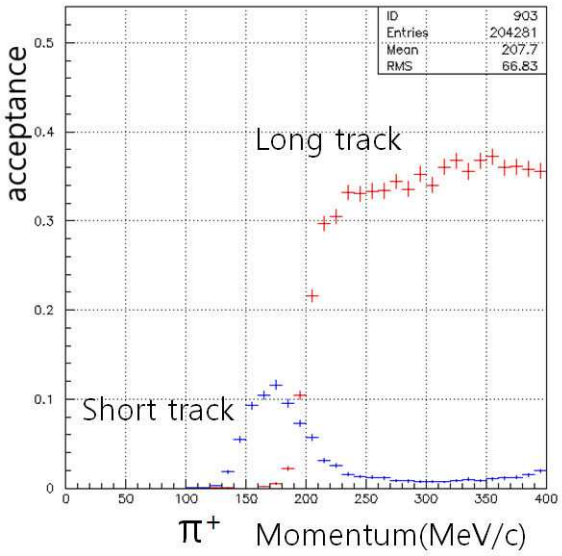

Figure 2.8: Geometrical acceptance for short track(blue) and long track(red) of π^+.

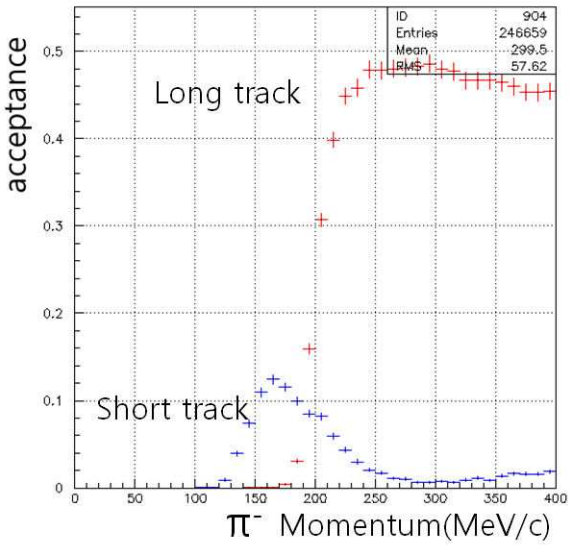

Figure 2.9: Geometrical acceptance for short track(blue) and long track(red) of π^-.

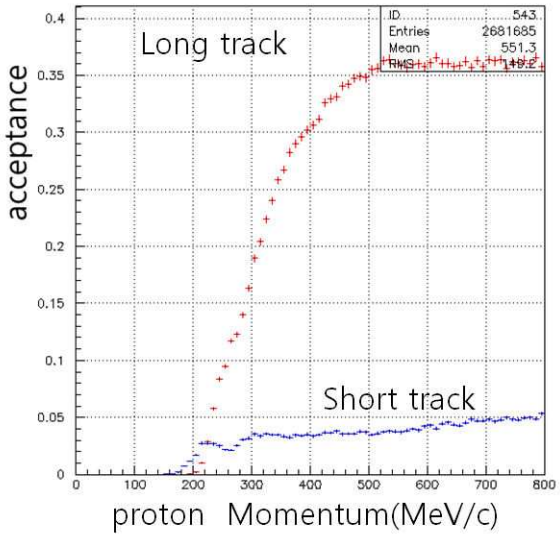

Figure 2.10: Geometrical acceptance for short track(blue) and long track(red) of proton in momentum scale.

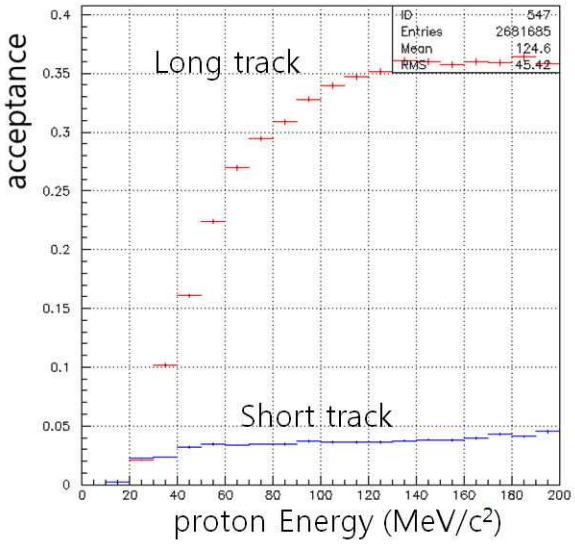

Figure 2.11: Geometrical acceptance for short track(blue) and long track(red) of proton in energy scale.

Chapter 3

Data Analysis

In this chapter, procedures of data analysis from the raw data are described.The analysis stage is divided into two parts: π^- spectra from the $(K^-_{stopped}, \pi^-)$reaction and "decay product part"to obtain the proton energy spectra of hypernuclei in the mehod of two tracks coincidence.

3.1 Λ hypernuclear production

3.1.1 Primary Beam

When e^+ beams(510MeV) collide e^- beams(510MeV), $\phi(1020)$ mesons are produced at a rate $4.4 \times 10^2 s^{-1}$. The $\phi(1020)$ decays with each branch ratio as shown.

$\phi \rightarrow K^+K^-$ (49%)
$\rightarrow K_SK_L$ (34%)
$\rightarrow \rho\pi + \pi^+\pi^-\pi^0$ (15%)

Since the ϕ is produced almost at rest, DAΦNE is a source of $2.2 \times 10^2 K^+K^-$ pairs/s, collinear, background free and of very low energy (16MeV). The low energy of the kaons is the key-feature for performing hypernuclear physics experiments at the DAΦNE ϕ-factory.

3.1.2 π^- in K^- absorption at rest

The main idea of FINUDA is to slow down to rest the negative kaons from the $\phi \rightarrow K^+K^-$ decay in thin solid target, so as to study the following formation and decay of hypernuclei produced by the strangeness exchange reation. Especially we choose the carbon targets(1,5,8)

$$K^-_{Stopped} + {}^{12}C \rightarrow {}^{12}_{\Lambda}C + \pi^- \tag{3.1}$$

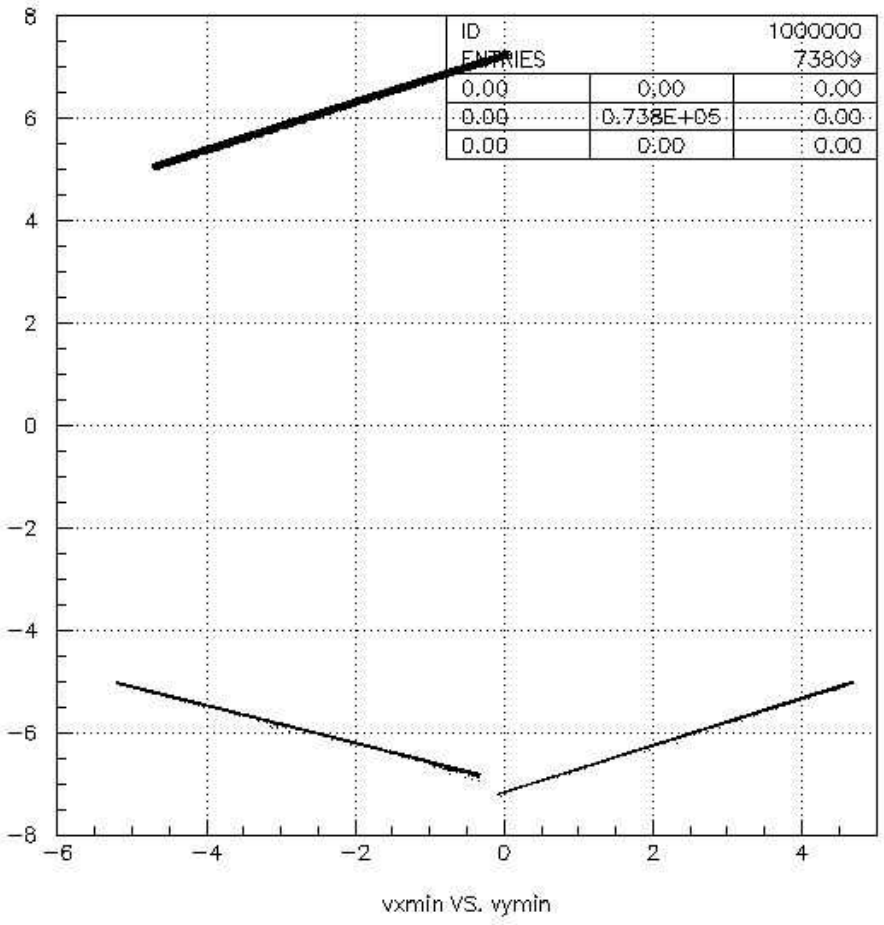

Figure 3.1: K^- stopping point in Carbon targets(1,5,8)

Figure 3.1 shows a K^- stopping points in Carbon targets. And in stopping point π^- are generated by each reaction.

$$K^-_{Stopped} + p \rightarrow \Sigma^- + \pi^- \tag{3.2}$$

$$K^-_{Stopped} + n \rightarrow \Sigma^0 + \pi^- \tag{3.3}$$

$$K^-_{Stopped} + n \rightarrow \Lambda + \pi^- \tag{3.4}$$

$$K^-_{Stopped} + p \rightarrow \Sigma^- + \pi^+ \ , \ \Sigma^- \rightarrow n + \pi^- \tag{3.5}$$

$$K^-_{Stopped} \ (NN) \ \Sigma^- \ N \ , \ \Sigma^- \rightarrow n + \pi^- \tag{3.6}$$

The analysis of the data started with a study of the excitation energy spectrum ${}^{12}_{\Lambda}C$, trying to maximize the instrumental resolution on the measurement of the π^- momenta. To that purpose the following requirements were adopted in the condition of a negative track (negative pion candidate) connected th the K^- stopping point and quality cut on the track fitting.

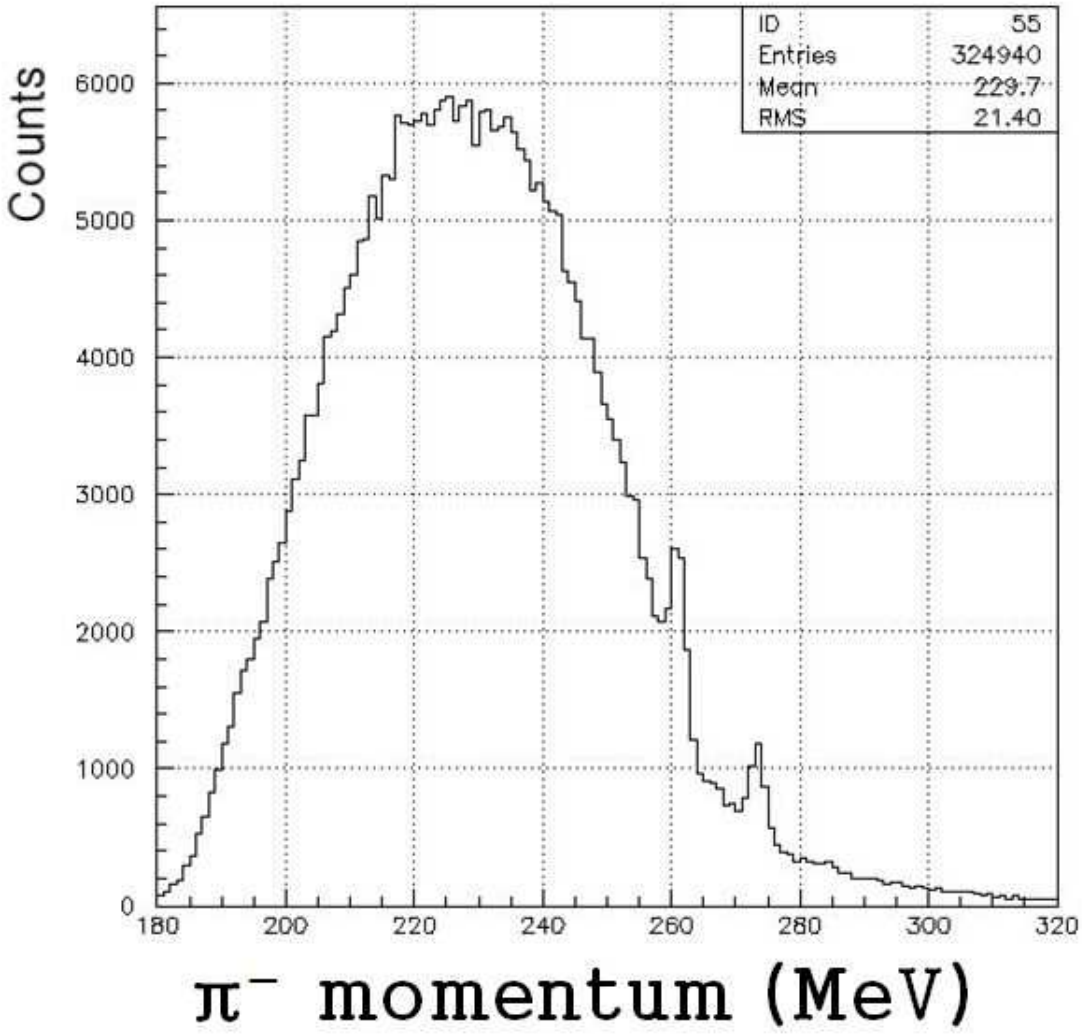

Figure 3.2: Inclusive momentum spectrum of π^- from ^{12}C targets obtained using more relaxed selection criteria.

3.2 Decay product part

From the NMWD of Λ hypernuclei, protons and neutrons are produced. For the decay particle analysis, it is important to identify charged product and neutral product.

In the next section, charged product, proton analysis will be described in the method of two track coincidence.

3.2.1 two track coincidence

Two track coincidence means that during gate time (18ns) both (+)charged particles and (-)charged particles are tracked at the stopping point. Figure 3.3 shows each (+) charged particle and (-) charged particle trace at the K^- stopping point.

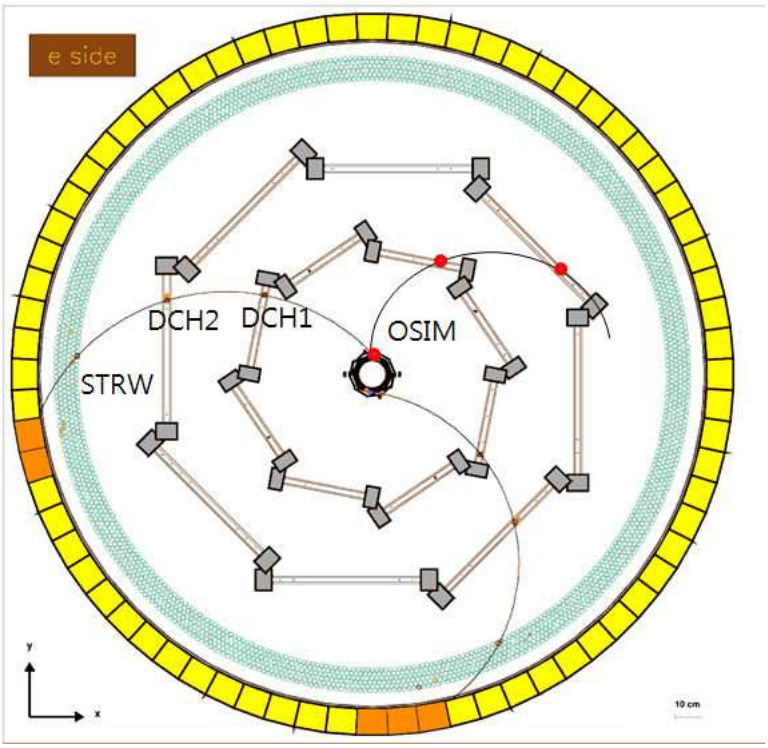

Figure 3.3: tracking two different charged particle at the stopping point.

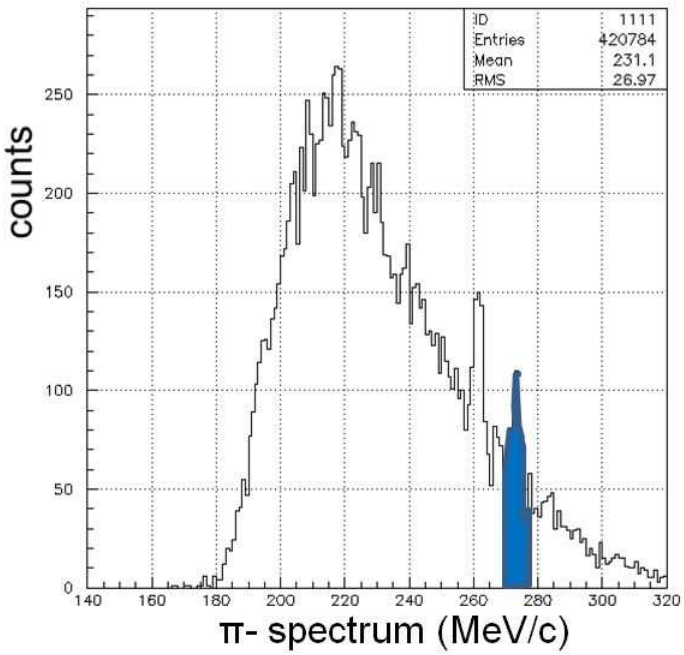

Figure 3.4: Momentum spectrum of π^- of fig. 3.2 with the additional requirement of a proton in coincidence. blue areas are ground state of π^-(270-277)MeV

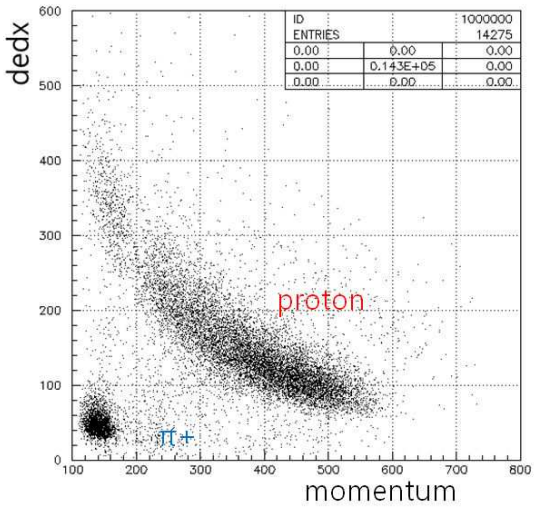

Figure 3.5: (+)charged particle pid.

3.2.2 Proton spectra from $^{12}_{\Lambda}$C ground state decay

$$\mathrm{K}^{-}_{Stopped} + {}^{12}\mathrm{C} \rightarrow {}^{12}_{\Lambda}\mathrm{C} + \pi^{-},$$
$$\Lambda + p \rightarrow p + n + 176 \text{ MeV}.$$

The ground state Λ are formed by release of 270-277 π^- momentum. Fig 3.6 show 4-point raw proton spectrum from non-mesonic weak decay of ground state . Event numbers are 404. Fig 3.7 included short track. Therefore proton event detected at the low energy.

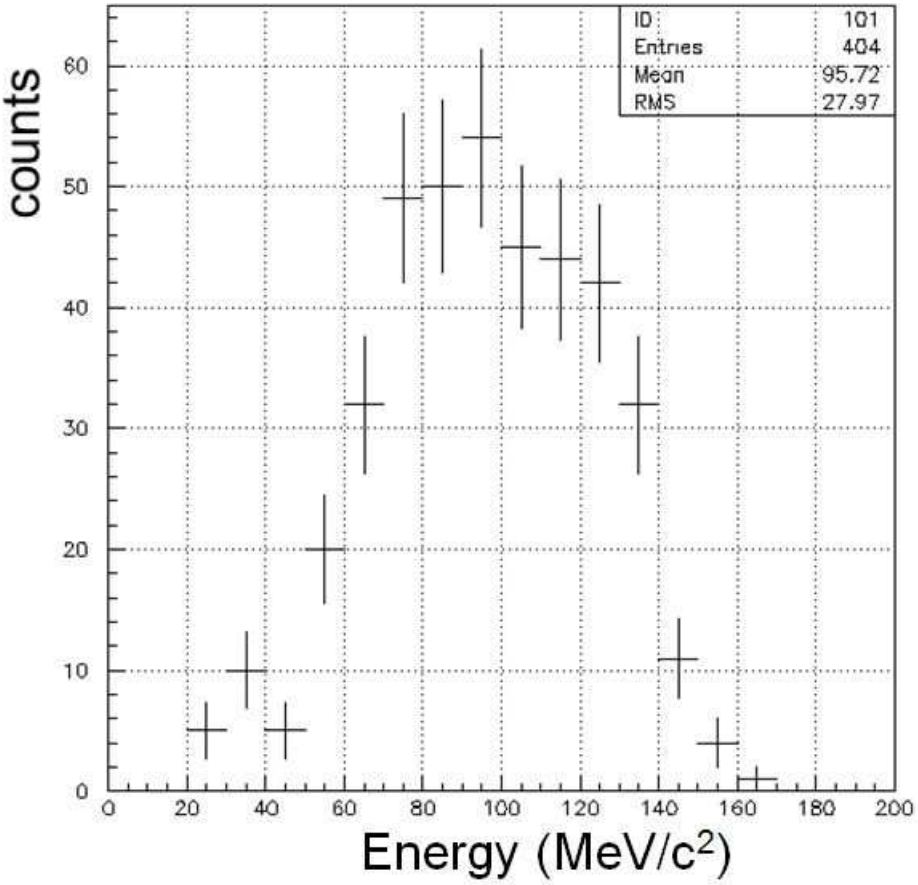

Figure 3.6: 4-point raw proton energy spectrum at the ground state with π^- coincidence (270-277gate).

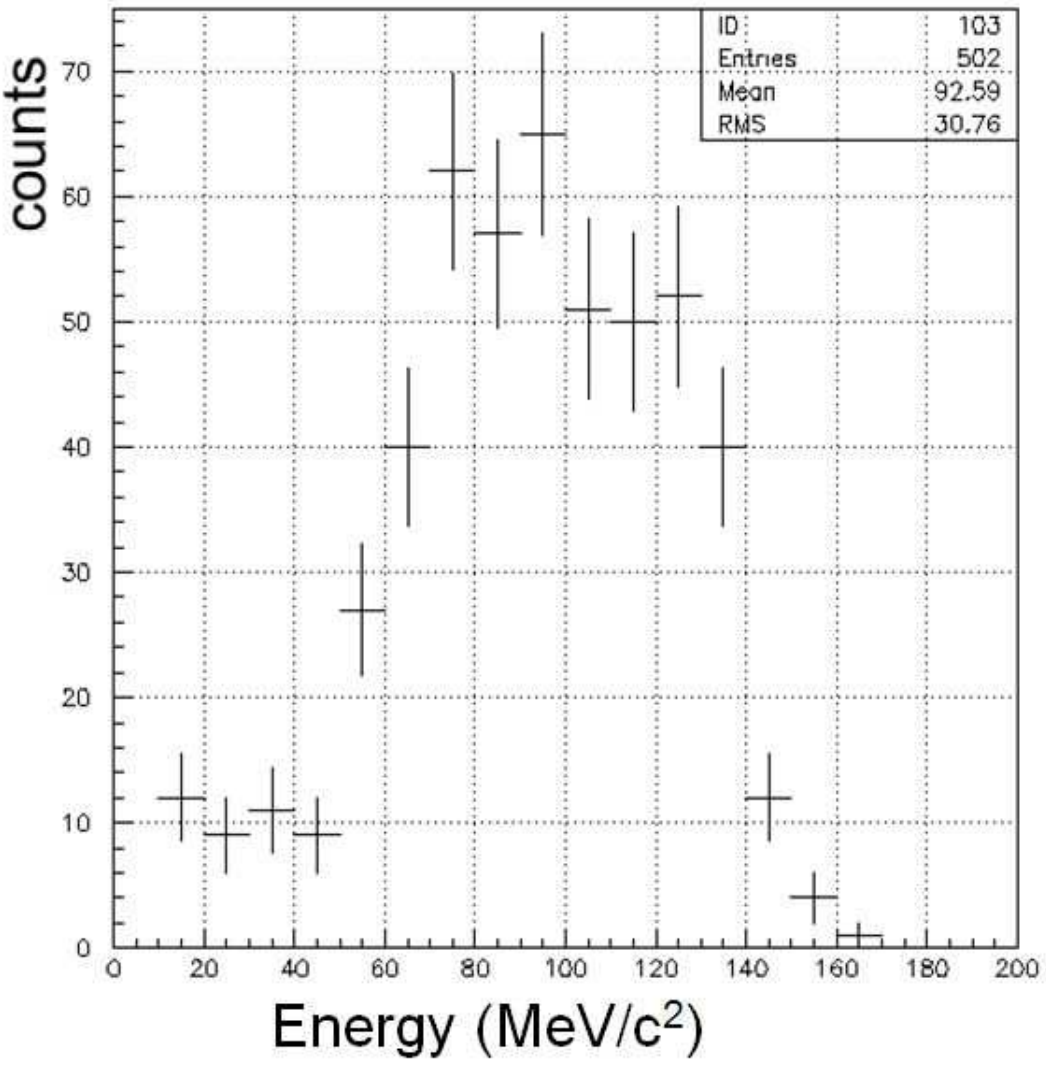

Figure 3.7: 3 or 4 point raw proton energy spectrum at the ground state with π^- coincidence(270-277gate).

Chapter 4

Results

In this chapter, we'll discuss about proton energy spectra after nonmesonic weak decay of Λ. In order to NMWD proton spectra, we estmated background region and corrected geometrical acceptance. And then we obtained proton energy spectra per NMWD assuming the total numbers of hypernuclues.

4.1 Proton energy spectra

From Fig 3.7, we have obtained proton spectra including long track and short track.

4.1.1 Background estimation

In order to obtain background, we assumed that background in the 270-277(MeV) π^- (ground states) is average between 265-270 (MeV) and 277-282 (MeV) π^-. The number of 265-270 (MeV) π^- are 199. The number of 277-282 (MeV) π^- are 315. we obtained 347 background numbers through fitting method 1 polynomial and 2 gaussian. Therefore total background events from both side bin were normalized by 347 events.

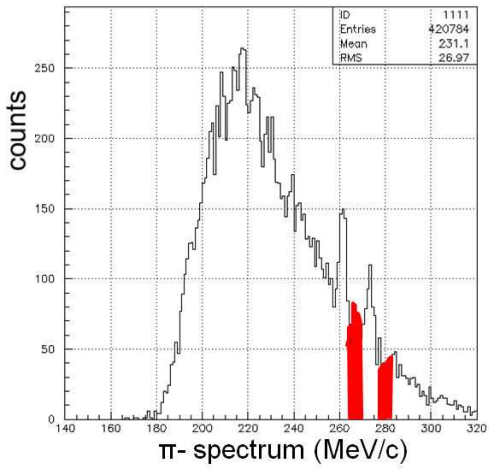

Figure 4.1: background estimation the region of 265-270 and 277-282 MeV π^- momentum

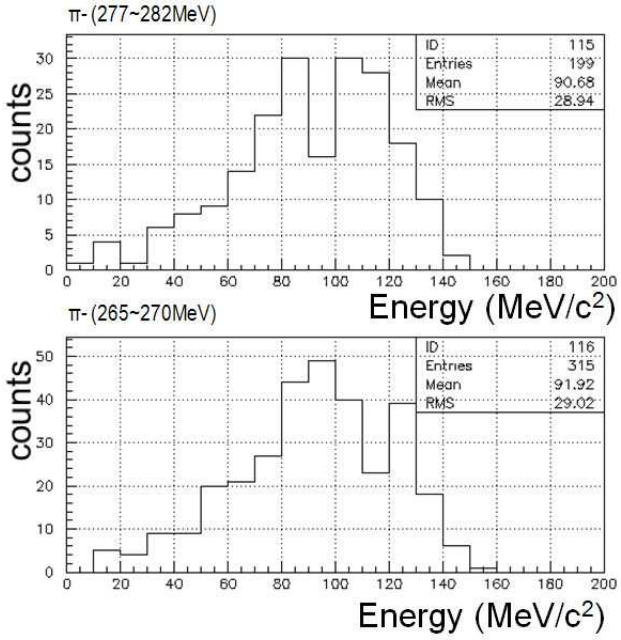

Figure 4.2: background proton spectrum with coincidence 265-270 and 277-282 MeV π^- momentum

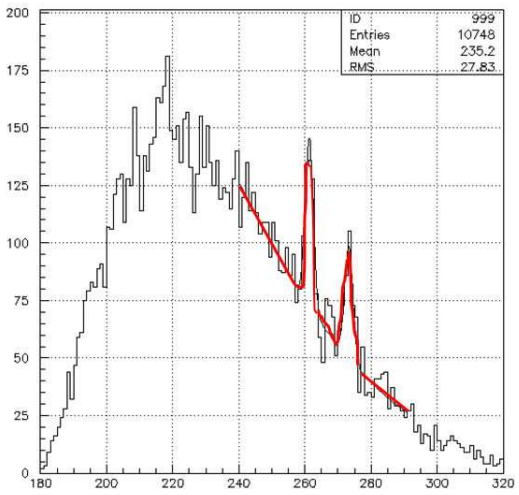

Figure 4.3: estimate background number,1-p2 polynominal and 2-gaussian fitting

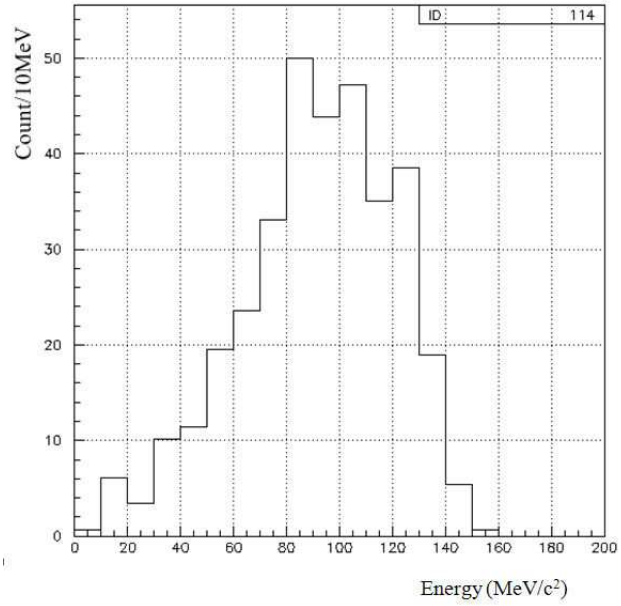

Figure 4.4: 347-background proton energy spectrum

4.1.2 Normalization and background subtraction

Fig 4.5 are subtracted raw proton spectrum. The error bars are the statistical errors. Fig 4.6 are proton spectrum after geometrical acceptance correction. The error calculation are as follow.

Error of a Difference: u = x - y

$\sigma_u^2 = \sigma_x^2 + \sigma_y^2$ - 2cov(x,y)

Error or a Ratio: u = x/y

σ_u^2 / $u^2 = \sigma_x^2/x^2 + \sigma_y^2/y^2$ -2cov(x,y)/xy

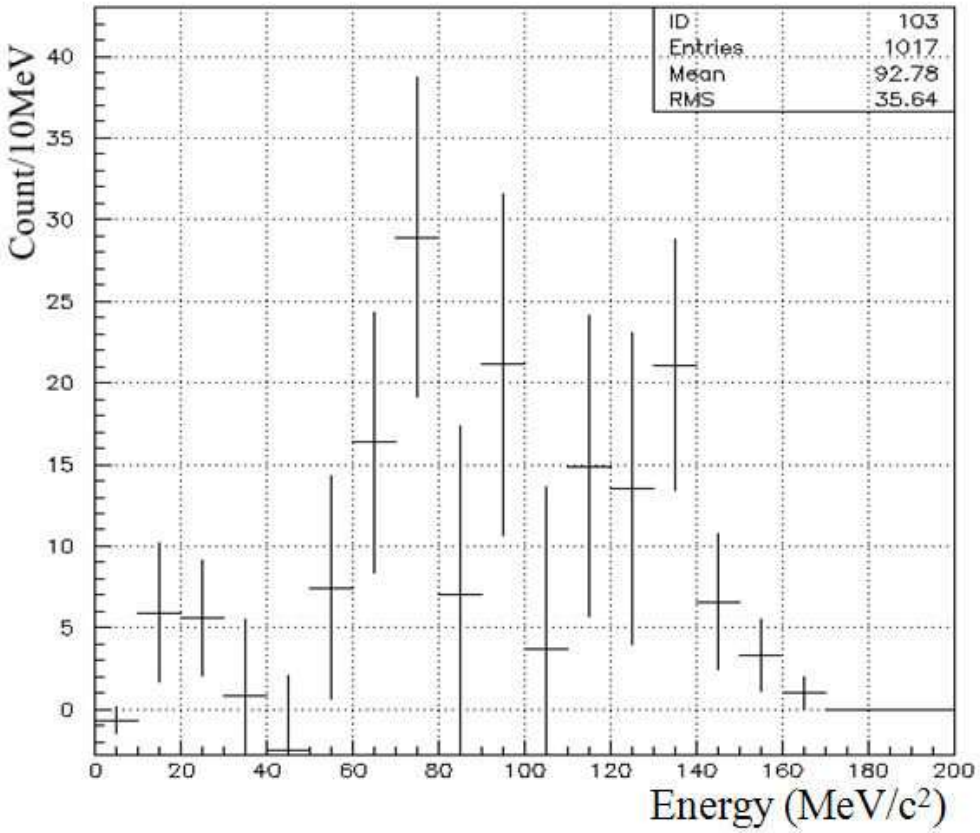

Figure 4.5: proton spectra after subtraction of the background.

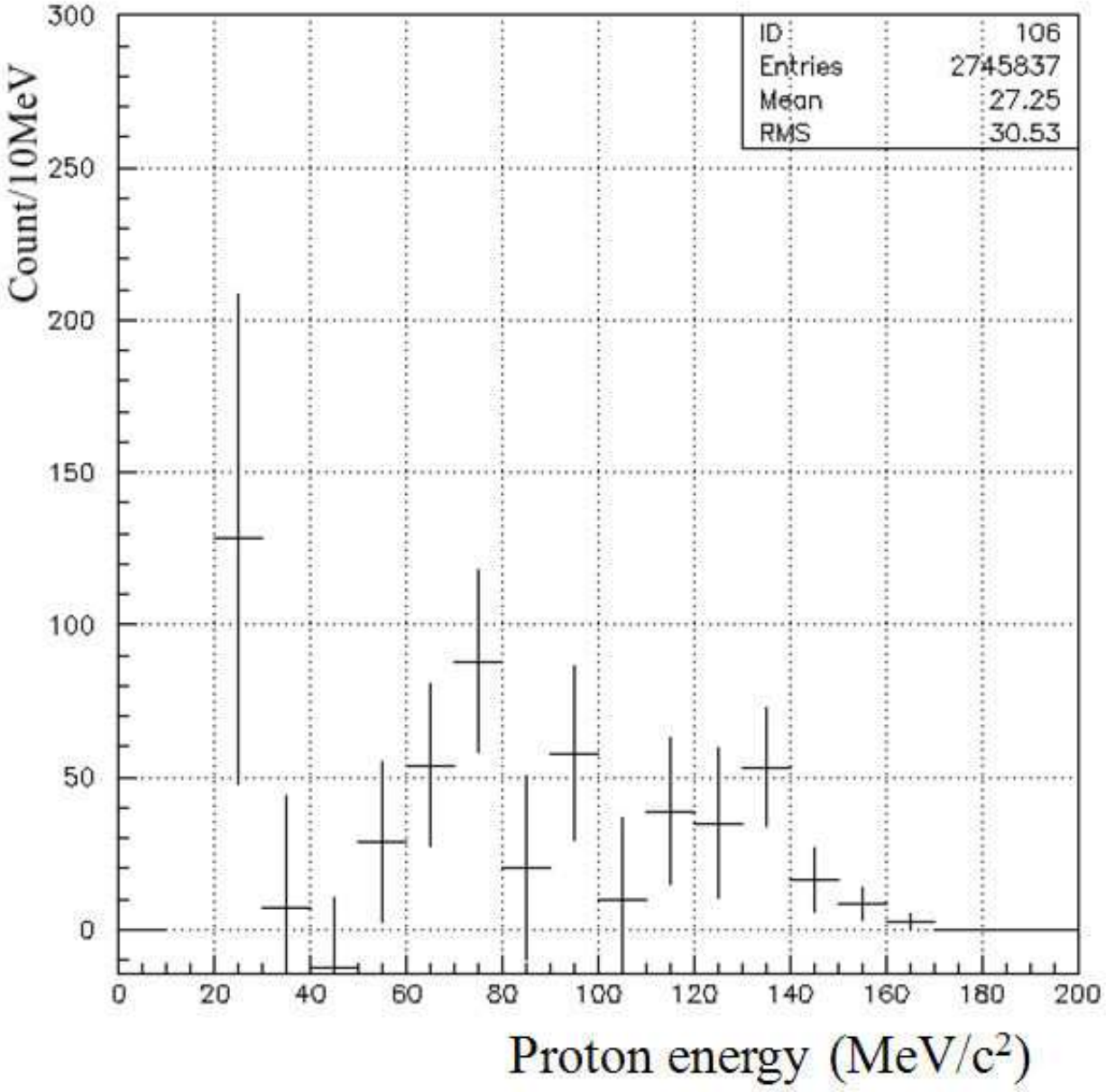

Figure 4.6: proton spectra after geometrical acceptance correction. The error bars are the statistical errors.

Table 4.1: Summary of the π^-, and NMWD branching ratios of in the E508.

		Ref.
b_{π^-}	$0.099 \pm 0.011 \pm 0.004$	[59]
b_{π^0}	$0.133 \pm 0.005 \pm 0.003$	[85]
b_{nm}	$\mathbf{0.768 \pm 0.012 \pm 0.005}$	[85]

4.1.3 Nonmesonic weak decay branching ratio

To convert the yield of the obtained nucleon energy spectra into the unit per NMWD, one need to know the absolute branch width of the NMWD. The NMWD width can be obtained by subtracting mesonic weak decay widths ($\Gamma_{\pi^-}/\Gamma_\Lambda$ and $\Gamma_{\pi^0}/\Gamma_\Lambda$) from as $\Gamma_{nm} = \Gamma_{tot} - \Gamma_{\pi^-} - \Gamma_{\pi^0}$, so that the NMWD branching ratio can be extracted from $b_{nm} = 1 - b_{\pi^0} - b_{\pi^-}$. Therefore, we also need to know the charged pion branch width as well. We took the data of this branch width from other analysis of E508[84, 85] for except for π^- branching ratio. The branching ratios of π^-, π^0 and NMWD branching ratios can be summarized in Table 4.1.

4.1.4 Proton energy spectra per NMWD

From the fig 4.8, we have obtained the proton energy spectra per NMWD. The number of π^-(270-277MeV) from formation of the Λ are 1387 through fitting method. From the table 4.1 applying the NMWd branch ratio, 0.768 the number of non-mesonic hypernucleus are 1065.

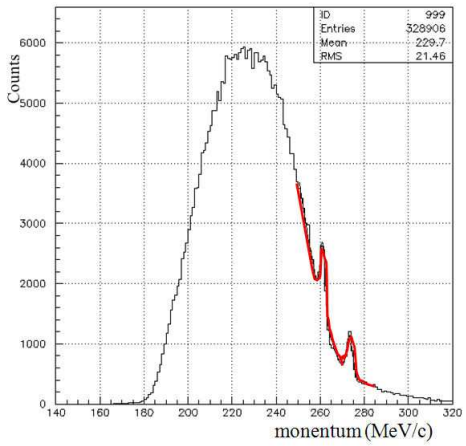

Figure 4.7: assuming hypernuclues from fitting

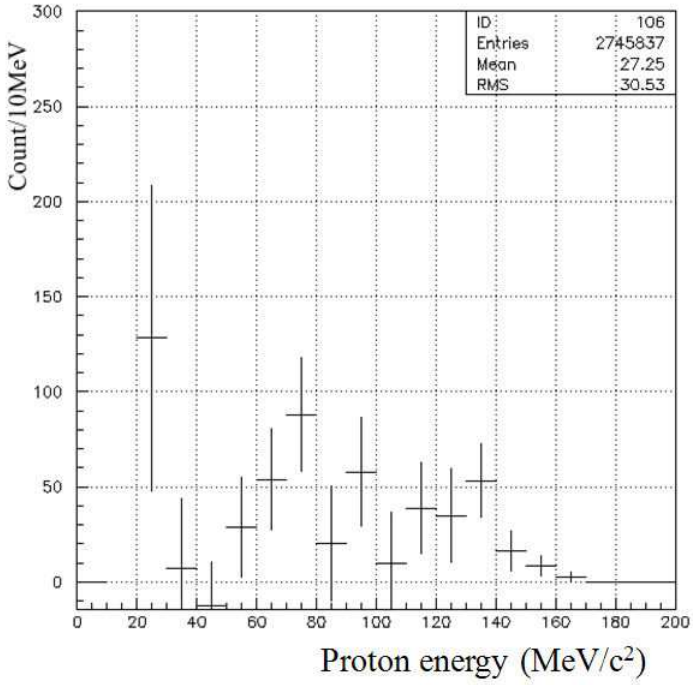

Figure 4.8: Proton energy spectra per NMWD of ${}^{12}_{\Lambda}$C

Chapter 5

Summary

In this thesis, I introduced the FINUDA experiment. In order to get the Γ_n/Γ_p ratio from non-mesonic weak decay, I have analyzed the proton energy spectrum from the non-mesonic weak decay of 12^{Λ}_{C} hypernucleus produced via (K^{-}_{stop}, π^{-}) reaction at FINUDA experiment.
I have obtained the proton yields in the low energy region below 30-40MeV for the first time. This was possible due to the thin target and better resolution of the FINUDA detector. The spectrum, counts per non-mesonic hypernucleus show a consistent yield in most of the energy region with that of the previous KEK-508 experiment except in the low energy region of 20-60 MeV. In order to improve the statistics, I have included the low energy short track events(98) in addition th those 4-point track(404). The spectrum shows the rapidly increasing yields as the proton energy decreases. contrasting the E508 experiment The reason is acceptance at the low energy. Therefore. I have obtained the acceptance of charged particle. The efficiency determination of the low energy proton is important.

In order to improve the statistics, we included the short track data in addition to the long-point data.

My result is different Benussi‘s result due to background subtraction. Whereas Benussi‘s background is peak at 110MeV with Monte Carlo simulation, I obtained 80Mev peak from side bin(265-270, 277-282) real data. Fig **??** is compared E508 and Finuda results.

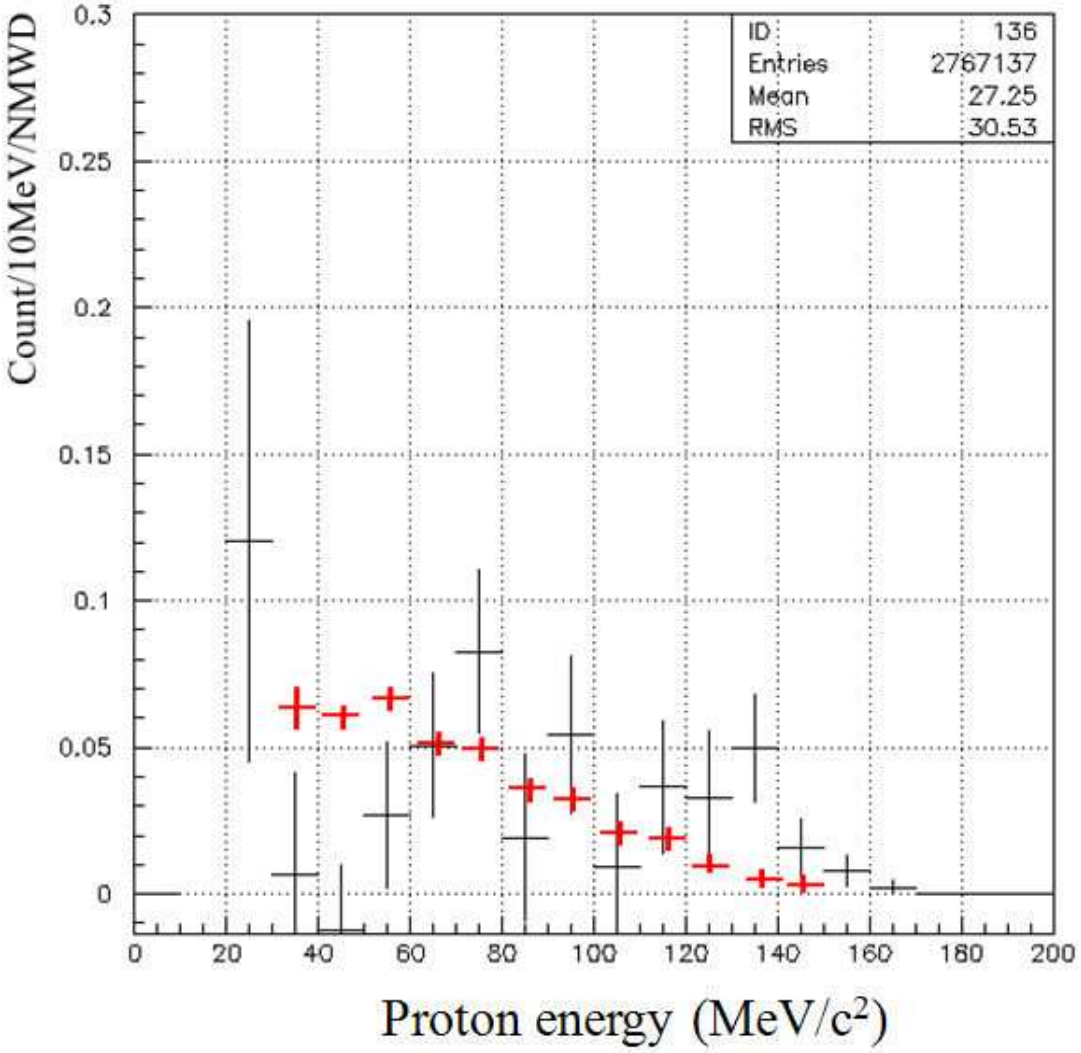

Figure 5.1: comparison between the Finuda(black) and E508(red) proton spectrum per NMWD

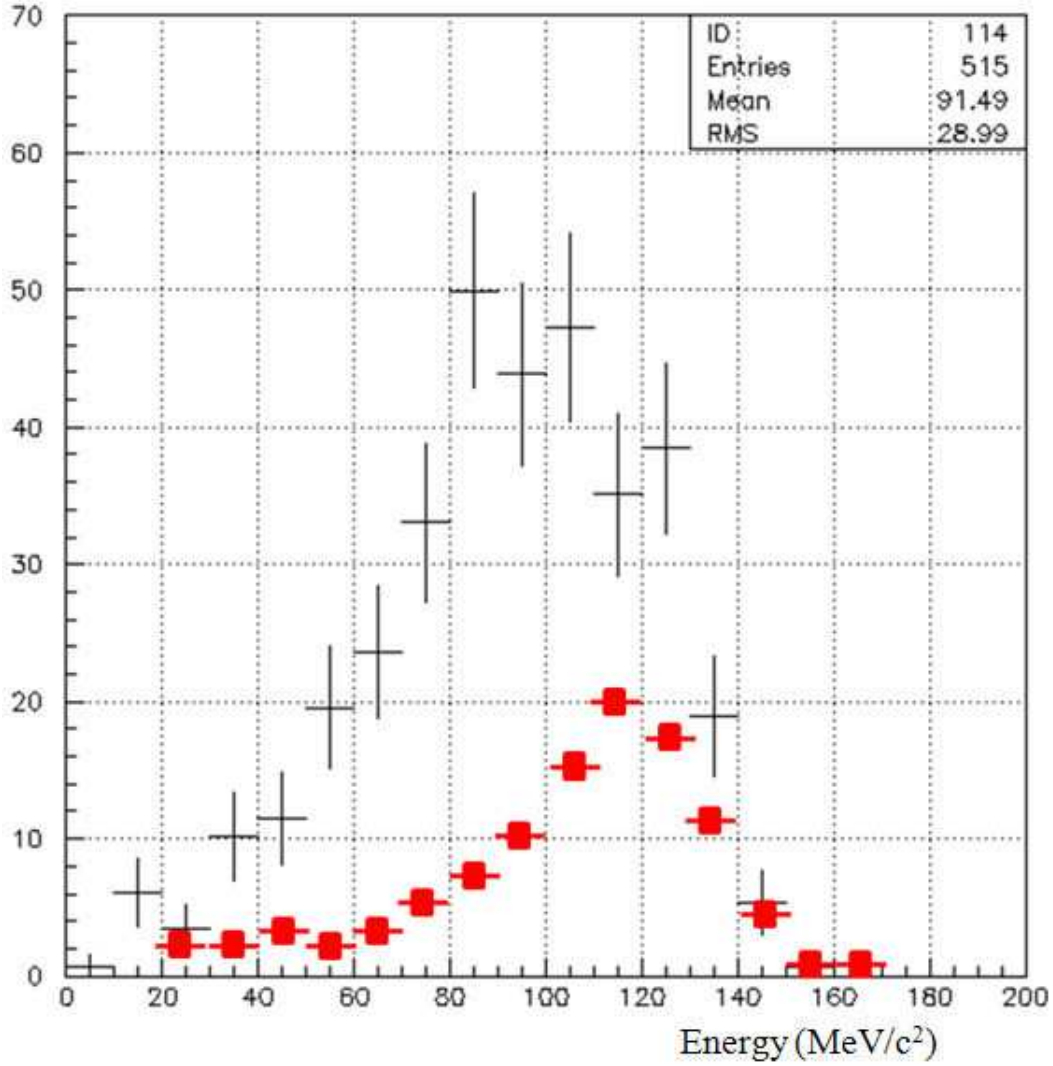

Figure 5.2: comparison background between Benussi MC(red square) and side bin data(black cross)

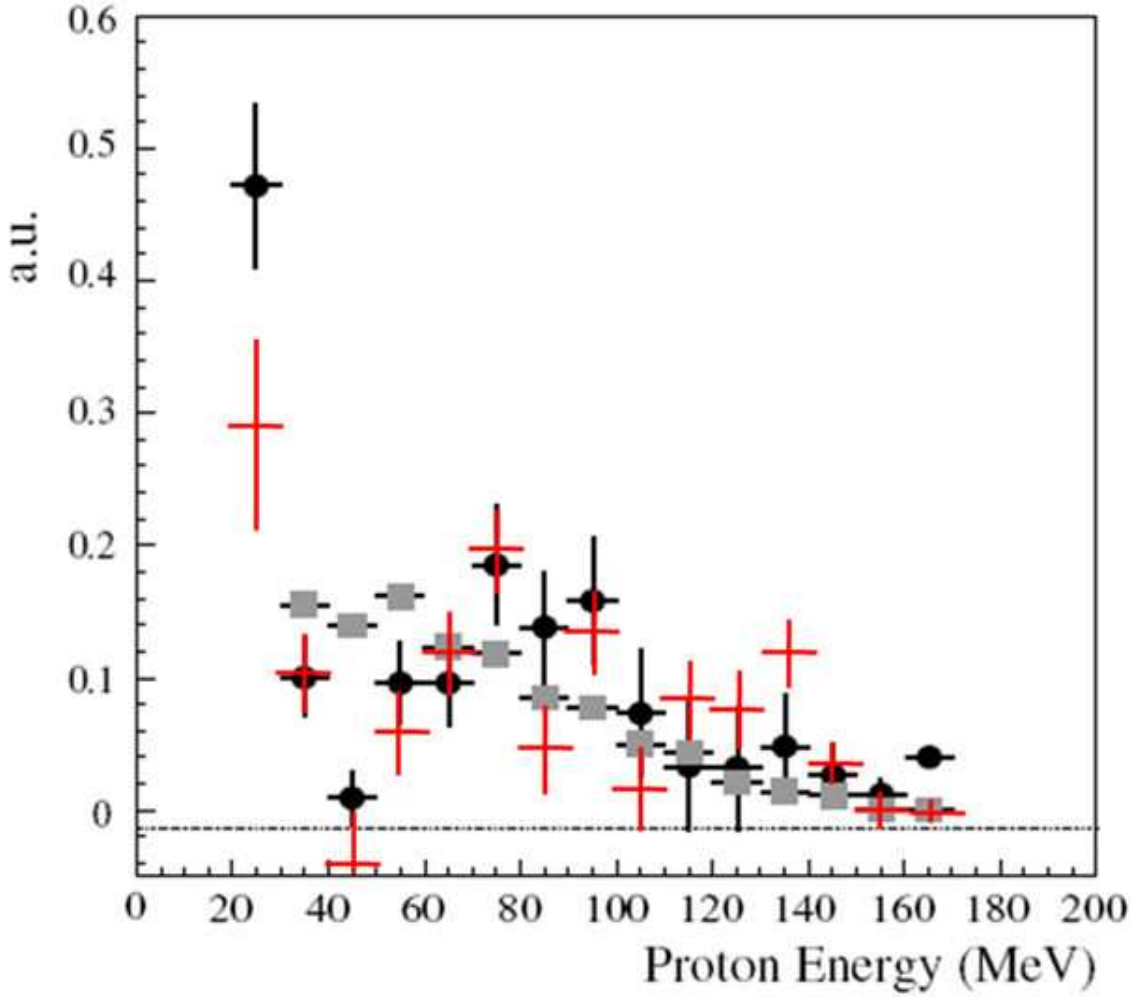

Figure 5.3: comparison among the Benussi(black) and E508(grey square) and YongJin(red) proton spectrum at a.u.

Bibliography

[1] B.R Martin and G. shaw, *Particle Physics* 2nd Edition, John Wiley & Sons, Chichester, (1997)

[2] N.Cabibbo, Phys. Rev. Lett.10 531 (1963)

[3] Outa.H.,Nuc. Phys. A639, 251c (1998)

[4] V.J.Zeps, *et al*, Nuc. Phys. A639, 261c (1998)

[5] J. Cohen, Phys. Rev. C42, 2724 (1990)

[6] Szymanski J., Phys. Rev. C43 849 (1991)

[7] M.Oka, Nuc. Phys. A639 317c (1998)

[8] K.Sasaki,Takashi Inoue,Makoto Oka, Nuc. Phys. A678 445 (2000)

[9] Kim J.H., *et al*, Presented at the Conference of Jap. Phys. Soc., Hiroshima, March (1999)

[10] Kim.M,J., Master Thesis, Seoul National Univ. (1997)

[11] K.A.Brueckner, R.Server, K.M.Watson, Phys. Rev. 84, 258(1951)

[12] Park.H,S., Ph.D. Thesis, Seoul National Univ. (1998)

[13] Kim.Y.D., *et al*, Nucl.Instr. and Meth A372, 431(1996)

[14] H.C.Chiang and J.Hüfner, Nucl. Phys. A352, 442(1981)

[15] S.Okada, Master thesis, Tokyo Inst. Tech.(2001)

[16] C.Cernigoi, N.Grion, G.Pauli and R.RuiR.CherubiniE.R.Gill, Nucl. Phys. A411, 382(1983)

[17] B.Bassalleck, H.D.Engelhardt, W.D.Klotz, F.Takeutchi, H.Ullrich and M.furic, Nucl. Phys. A319, 397(1979)

[18] R,Hartmann, H.P.Isaak, R.Engfer, E.A.Hermes, H.S.Pruys, W.Dey, J.J.Pfeiffer, U.Sennhauser, H.K.Walter and J.Morgenstern,, Nucl. Phys. A308, 345(1978)

[19] U.Klein, G.Büche, W.Kluge, H.Matthay and G.Mechtersheimer, Nucl. Phys. A329, 339(1979)

[20] H. Bandō, T. Motoba and J. Žofka, Int. Jour. Mod. Phys. A**5**, 4021 (1990).

[21] Part. Data Group, Eur. Phys. J. C**3**, (1998).

[22] J. Cohen, Prog. Part. Nucl. Phys. **Vol. 25**, 139 (1990).

[23] W. M. Alberico, A. De Pace, M. Ericson, and A. Molinari, Phys. Lett. B **256**, 134 (1991).

[24] A. Ramos, E. Oset, and L. L. Salcedo, Phys. Rev. C**50**, 2314 (1994).

[25] W. M. Alberico, G. Garbarino, Phys. Rep. **369**, 1-109 (2002), and references therein.

[26] H. Bandō and H. Takaki, Prog. Theor. Phys. **72**, 106(1984).

[27] T. Motoba, Nucl. Phys. A**547**, 115c (1992).

[28] J. F. Donoghue *et al.,* Phys. Rev. D**21,** 186 (1980).

[29] R. A. Schumacher, Nucl. Phys. A**547,** 143c (1992).

[30] K. Maltman and M. Shmatikov, Nucl. Phys. A**585**, 343c (1995); Phys. Rev. C**51,** 1576 (1995); Phys. Lett. B**331,** 1 (1994).

[31] T. Inoue, S. Takeuchi and M. Oka, Nucl. Phys. A**597,** 563 (1996)

[32] W. Cheston, H. Primakov, Phys. Rev. **92**, 1537 (1953)

[33] B. H. J. McKeller and P. Pick, Phys. Rev. D**6**, 2184 (1972); *ibid,* **7,** 2160 (1973); *ibid,* **8,** 265 (1973); A. P. Balanchandran *et al.,* Phys. Rev. **153,** 1553 (1967); J. C. Pati and C. H. Woo, Phys. Rev. D**3,** 2920 (1971); K. Muira and T. Minamikawa, Prog. Theor. PHys. **38,** 954 (1967); M. A. Shifman *et al.,* Nucl. Phys. **20,** 315 (1977); W. A. Bardeen *et al.,* Phys. Lett. B**191,** 138 (1987), Nucl. Phys. B**293,** 787 (1988).

[34] J. B. Adams, Phys. Rev. **156**, 1611 (1967).

[35] B. H. McKellar and B. F. Gibson Phys. Rev. C**30** 3223 (1984).

[36] K. Takeuychi, H. Takaki and H. Bando Prog. Theor. Phys. Vol.**73** 841 (1985).

[37] H. Bando, T. Motoba and J. Zofka Inter. Journ. Mod. Phys. A Vol.**5** No.21 4021-4198 (1990).

[38] J. F. Dubach Nucl. Phys. A**450**, 71c (1986).

[39] A. Parreño, A Ramos and C. Bennhold Phys. Rev. C**56**, 339 (1997).

[40] A. Parreño and A. Ramos, Phys. Rev. C **65**, 015204 (2001)

[41] K. Itonaga, T. Ueda, and T. Motoba, Nucl. Phys. A**577**, 301c (1994). K. Itonaga, T. Ueda, and T. Motoba, Nucl. Phys. A**585**, 331c (1995).

[42] K. Itonaga, T. Ueda and T. Motoba, Nucl. Phys. A**585**, 331c (1995).

[43] M. Shmatikov, Nucl. Phys. A**580**, 538 (1994).

[44] K. Itonaga *et al.*, Phys. Rev. C **65**, 034617 (2002).

[45] D. Jido, E. Oset and J. E. Palomar, Nucl. Phys. A **694**, 525 (2001).

[46] C.-Y. Cheung, D. P. Heddle and L. S. Kisslinger, Phys. Rev. C**27**, 335 (1983).

[47] D. P. Heddle and L. S. Kisslinger Phys. Rev. C**33** 608 (1986).

[48] T. Inoue, M. Oka, T. Motoba and K. Itonaga, Nucl. Phys. A**633,** 312 (1998).

[49] K. Sasaki, T. Inoue, and M. Oka, Nuc. Phys. A **669**, 331 (2000).

[50] W. M. Alberico, A. De Pace, G. Garbarino, and A. Ramos, Phys. Rev. C **61**, 044314 (2000).

[51] A. Ramos and C. Bennhold, Nucl. Phys. A **577**, 287c (1994).

[52] A. Parreño and A. Ramos and C. Bennhold, Phys. Rev. C**52**, R1768 (1995). Erratum: A. Parreño and A. Ramos and C. Bennhold, Phys. Rev. C**54**, 1500 (1996)

[53] J. F. Dubash, G. B. Feldman and B. R. Holstein, Ann. Phys. **249**, 146 (1986)

[54] A. Parreño and A. Ramos, C. Bennhold and K. Maltman, Phys. Lett. B **435**, 1 (1998).

[55] A. Parreño and A. Ramos, Phys. Rev. C**65**, 015204 (2002).

[56] K. Itonaga, T. Ueda, and T. Motoba Nucl. Phys. A**639,** 329c (1998).

[57] J.-H. Jun and H. C. Bhang, Nuovo Cimento A 112 649 (1999)
J.-H. Jun, Phys. Rev. C **63**, 044012 (2001)

[58] J. J. Szymanski *et al.*, Phys. Rev. C **43**, 849 (1991).

[59] Y. Sato *et al.*, Phys. Rev. C **71**, 025203 (2005)

[60] O. Hashimoto *et al.*, Phys. Rev. Lett. **88**, 042503 (2002).

[61] A. Ramos, M. J. Vicente-Vacas and E. Oset, Phys. Rev. C**55**, 735 (1997).

[62] A. Ramos, M. J. Vicente-Vacas, and E. Oset, Phys. Rev. C **66** 039903(E) (2002).

[63] J. H. Kim *et al.*, Phys. Rev. C**68**, 065201 (2003).

[64] H. Noumi *et al.* Phys. Rev. C**52**, 2936 (1995).

[65] H. Outa *et al.* Nucl. Phys. A**639**, 251c (1998).

[66] V.J. Zeps *et al.* Nucl. Phys. A**639**, 261c (1998).

[67] H. Outa *et al.* Nucl. Phys. A**585**, 109c (1995).

[68] H. Outa, KEK PS experiment E462 (2000).

[69] R. Bertini , Nucl. Phys. A **368**, 365 (1981).

[70] S. Ajimura , Phys. Rev. Lett. **84**, 4052 (2000).

[71] K. H. Tanaka *et al.*, Nucl. Phys. A **450**, 533c (1986).

[72] T. Fukuda *et al.*, Nucl. Instr. and Meth. A **361**, 485 (1995).

[73] T. Shintomi *et al.*, IEEE Trans. on Magnetics, Mag**28**, 805(1992).

[74] T. Hasegawa *et al.* Phys. Rev. C **53**, 1210 (1996).

[75] T. Hasegawa *et al.*, Nucl. Instr. and Meth. A**342**, 383 (1994).

[76] Y. D. Kim *et al.*, Nucl. Instr. and Meth. A**372**, 431 (1996).

[77] H. Hotchi *et al.*, Phys. Rev. C **64**, 044302 (2001).

[78] J. Myrheim and L. Bugge, Nucl. Instr. and Meth. **160**, 43 (1979).

[79] T. Hasegawa, Doctor Thesis of Graduate school, University of Tokyo, INS-IM-15 (1994).

[80] T. Tanimori *et al.*, Nucl. Instr. and Meth. **216**, 57 (1983).

[81] J. B. Birks, Proc. Phys. Soc A**64**, 874 (1951).

[82] W. R. Leo, *Techniques for Nuclear and Particle Physics Experiments* (Springer-Verlag, 1992).

[83] Low energy particle simulator. developed by M. Iwasaki.

[84] S. Kameoka *et al.*, Nucl. Phys. A **754**, 173 (2005).

[85] S. Okada *et al.*, Nucl. Phys. A **754**, 178 (2005).

[86] J. K. Dickens, ORNL-6436, Oak Ridge National Laboratory, (1988).

[87] R. A. Cecil, B. B. Anderson, and R. Madey, Nucl. Instrum. Methods **161**, 439 (1979).

[88] R. C. Byrd *et al.*, Nucl. Instrum. Methods A **313**, 437(1992).

[89] J. H. Kim, Doctor Thesis, Seoul National University (2003).

[90] G. Betti *et al.*, Nucl. Instrum. Methods **135**, 319 (1976).

[91] G. Garbarino, A. Parreño and A. Ramos, Phys. Rev. Lett. **91**. 112501 (2003).

[92] G. Garbarino, A. Parreño and A. Ramos, Phys. Rev. C. **69**. 054603 (2004).

[93] H. Bhang, M. J. Kim and J. H. Kim, AIP. Conf. Proc **594**, 171 (2001).

[94] S. Okada *et al.*, Phys. Lett. B**597**, 249 (2004).

[95] A. Sakaguchi *et al.* Phys. Rev. C **43**, 73 (1991)

[96] K. Sasaki, T. Inoue and M. Oka, Nucl. Phys. A **669**, 331 (2000); Nucl. Phys. A **678**, 455 (2000).

[97] B. H. Kang *et al.* , accepted to Phys. Rev. Letters and appeared in nucl-ex/0509015.

[98] C. Bennhold and A. Ramos, Phys. Rev. C **45**, 3017 (1992).

[99] T. Maruta *et al.* ,Nucl. Phys. A **754**, 168c (2005) and appeared in nucl-ex/0509016.

[100] S. Ajimura *et al.* , Phys. Lett. B **282**, 293 (1992).

[101] K. Sasaki, T. Inoue and M. Oka, Nucl. Phys. A **691**, 201 (2001).

[102] A. Sakaguchi *et al.* ,Phys. Rev. C **43**, 73 (1991)

[103] B. H. Kang, Ph. D. Thesis, Seoul National University, 132 (2004).

[104] M. J. Kim *et al.* , Journal of the Korean Physical Society, Vol. **46**, No. 4. 805 (2005).